Superconductivity and normal state properties of non-centrosymmetric CePt$_3$Si: a status report

E. Bauer

Institut für Festkörperphysik, Technische Universität Wien, A-1040 Wien, Austria
E-mail: ernst.bauer@ifp.tuwien.ac.at

I. Bonalde

Centro de Fisica, Instituto Venezolano de Investigaciones Cientificas,
Apartado 21874, Caracas, 1020-A, Venezuela

M. Sigrist

Theoretische Physik, ETH-Hönggerberg, 8093 Zürich, Switzerland

Ternary CePt$_3$Si crystallizes in the tetragonal *P4mm* structure which lacks a center of inversion. Antiferromagnetic order sets in at $T_N \approx 2.2$ K followed by superconductivity (SC) below $T_c \approx 0.75$ K. Large values of $H'_{c2} \approx -8.5$ T$/$K and $H_{c2}(0) \approx 5$ T were derived, referring to Cooper pairs formed out of heavy quasiparticles. The mass enhancement originates from Kondo interactions with a characteristic temperature $T_K \approx 8$ K. CePt$_3$Si follows the general features of correlated electron systems and can be arranged within the Kadowaki−Woods plot next to the unconventional SC UPt$_3$. NMR and μSR results show that both magnetic order and SC coexist on a microscopic scale without having spatial segregation of both phenomena. The absence of an inversion symmetry gives rise to a lifting of the degeneracy of electronic bands by spin-orbit coupling. As a consequence, the SC order parameter may have uncommon features as indicated from a very unique NMR relaxation rate $1/T_1$ and a linear temperature dependence of the penetration depth λ.

1. Introduction

Electron correlations in solids are a «magic door» to the discovery of unexpected features and phases of metals, intermetallics and oxides at low temperatures. Of particular importance are phase transitions at $T = 0$. Critical fluctuations associated with such a phase transition can lead to strong renormalization of normal metallic properties and novel exotic phases may emerge from these strongly fluctuating environments. One of the most exciting features in this context is the occurrence of superconductivity (SC).

The appearance of SC in such a scenario can deviate from the common BCS type in many essential aspects. Strong correlation effects responsible for the heavy electron behavior from narrow *f*-electron bands, may hamper the possibility of conventional Cooper pairing, i.e. pairing in the most symmetric (*s*-wave) form as it is favoured by electron−phonon interaction. In turn, magnetic fluctuation may provide the necessary attractive interaction in a different angular momentum channel. This means that Cooper pairs may have either spin−singlet or spin−triplet configuration and the orbital angular momentum may lead to a highly anisotropic gap with zero nodes. Almost all previously studied SC exhibiting strong electron correlations in the normal state region are characterized by a center of inversion in its crystal structure. This allows us to distinguish spin−singlet and spin−triplet components of the SC order parameter and consider them separately. Superconductivity in materials having no inversion symmetry is rare. This lack of a inversion center invalidates some aspects of the scheme of symmetry classification and leads to a mixture of singlet and triplet pairing in general.

A recently discovered example in this respect is CePt$_3$Si with the tetragonal space group *P4mm* (No. 99) [1], the first heavy fermion SC without a centre of inversion. The absence of inversion symmetry induces peculiar band splittings, as we will discuss below, which are detrimental to certain kinds of Cooper pairing channels. In particular, spin triplet pairing becomes unlikely under these circumstances [2].

The aim of the present paper is to provide a review of results of current research dedicated to the various physical properties of CePt$_3$Si in both the normal and superconducting states and to locate the system in the standard generic phase diagram of heavy fermion compounds.

This paper is organized as follows. After a discussion of normal state properties of CePt$_3$Si, the SC features of CePt$_3$Si are examined before theoretical considerations concerning the SC order parameter are made.

2. Results and discussion

2.1. Normal state properties

Physical properties of ternary CePt$_3$Si are dominated by the onset of long range, presumably antiferromagnetic order below $T_N \approx 2.2$ K, followed by SC below $T_c = 0.75$ K. This intriguing coincidence of two ordering phenomena in CePt$_3$Si have to be considered in the context of crystal electric field (CEF) splitting and Kondo interaction which substantially modify Hund's $j = 5/2$ ground state of the Ce ion.
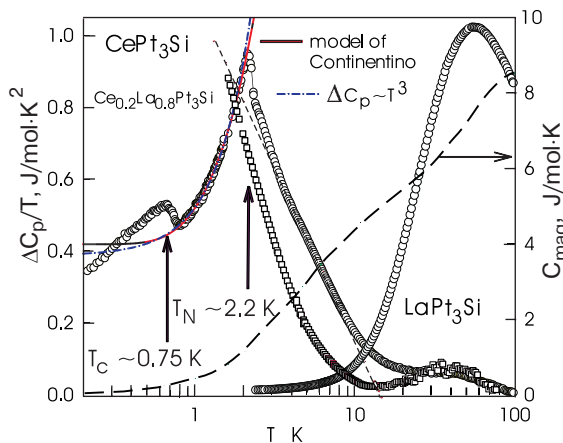

Fig. 1. Temperature dependent magnetic contribution to the specific heat, ΔC_p of CePt$_3$Si plotted as $\Delta C_p/T$ on a logarithmic temperature scale (filled circles). The phonon contribution to define ΔC_p is taken from $C_p(T)$ of LaPt$_3$Si (filled diamonds). The long-dashed line represents the magnetic entropy (right axis). The short-dashed line is a guide to the eyes and roughly indicates the non-Fermi liquid behavior. The solid line is a fit according to Eq. (1) and the dashed-dotted line is a fit according to $\Delta C_p \sim T^3$.

The response of the system associated with the mutual interplay of these mechanisms will be highlighted below.

Substantial information concerning the magnetic and the paramagnetic properties of CePt$_3$Si can be deduced from the temperature dependent magnetic contribution to the specific heat $C_{\mathrm{mag}}(T)$. The latter may be defined by the difference ΔC_p between CePt$_3$Si and isostructural non-magnetic reference LaPt$_3$Si, with $\Delta C_p \sim C_{\mathrm{mag}}$. Plotted in Fig. 1 is $\Delta C_p/T$ vs. T of CePt$_3$Si together with the raw data of LaPt$_3$Si. The low temperature behavior of the latter can be accounted for in terms of the Debye model with $\theta_D = 255$ K together with a Sommerfeld value $\gamma \approx 9$ mJ$/$mol$\cdot$K^2. $\Delta C_p(T)$ of CePt$_3$Si defines three regimes: the SC state of CePt$_3$Si below $T_c = 0.75$ K; the magnetically ordered range below $T_N \approx 2.2$ K and the paramagnetic region above T_N. This region is characterized by a Schottky-like anomaly with a weak local maximum around 40 to 50 K. Such numbers imply a CEF level approximately 100 K above the ground state doublet. However, since $C_p(T)$ of LaPt$_3$Si slightly exceeds the specific heat data of CePt$_3$Si, $\Delta C_p(T) \sim C_{\mathrm{mag}}(T)$ becomes negative, hence a reliable evaluation of CEF level scheme is not possible, at least, considering this quantity only. The integrated entropy S_{mag} (right axis, Fig. 1) reaches $R\ln 2$ around 25 K and the entropy of 8.7 J$/$mol$\cdot$K^2 integrated up to 100 K is slightly less than $R\ln 4 = 11.5$ J$/$mol$\cdot$K^2. These results confirm again that the ground state of Ce^{3+} ions is a doublet with the first excited level above about 100 K. The twofold degeneracy of the ground state doublet, however, is lifted by magnetic order as well as by Kondo type interaction spreading entropy to higher temperatures.

The second interesting aspect in the paramagnetic temperature range of CePt$_3$Si is an almost logarithmic tail of $\Delta C_p/T$ above T_N, extrapolating to about 12 to 13 K. The logarithmic temperature dependence observed just above the magnetic transition may be considered as hint of non-Fermi liquid (nFl) behavior. Therefore, it is a unique observation at ambient pressure that non-Fermi liquid behavior, magnetic ordering and eventually a SC transition consecutively arises on the same sample upon lowering the temperature. To corroborate the nFl property deduced for CePt$_3$Si from the specific heat data and to exclude short range order effects and inhomogeneities above the magnetic phase transition, $C_p(T)$ was studied for diluted Ce$_{0.2}$La$_{0.8}$Pt$_3$Si as well. Results are shown in Fig. 1 as ΔC_p vs. $\ln T$ (squares). This diluted sample — without magnetic ordering — exhibits a similar logarithmic contribution to the specific heat, like parent CePt$_3$Si, and thus states this feature as intrinsic property.

In order to analyze in more detail the magnetically ordered region of CePt$_3$Si, a model by Continentino [3] is applied for the specific heat well below T_{mag}:

$$C_{mag}(T) = g\Delta_{SW}^{7/2} T^{1/2} \exp(-\Delta_{SW}/T) \times$$

$$\times \left[1 + \frac{39}{20}\left(\frac{T}{\Delta_{SW}}\right) + \frac{51}{32}\left(\frac{T}{\Delta_{SW}}\right)^2 \right]. \quad (1)$$

This expression is based on antiferromagnetic magnons with a dispersion relation $\omega = \sqrt{\Delta_{SW}^2 + D^2 k^2}$, where Δ_{SW} is the spin-wave gap and D is the spin-wave velocity; $g \propto 1/D^3 \propto 1/\Gamma^3$ and Γ is an effective magnetic coupling between the Ce ions. A least squares fit of Eq. (1) to the data below T_N (solid line, Fig. 1) reveals $\Delta_{SW} \approx 2.7$ K, a reasonable gap value with respect to the ordering temperature. A recent neutron diffraction study carried out on CePt$_3$Si confirmed antiferromagnetic ordering below $T_N \approx 2.2$ K with a wave vector $\mathbf{k} = (0,0,1/2)$, i.e. doubling of the magnetic unit cell along the **c**-direction [4]. A second model calculation with simple antiferromagnetic spin waves, yielding $C_{mag} \propto T^3$, gives again reasonable agreement with the heat capacity data. Using both models, one can estimate a Sommerfeld coefficient of 0.42 and 0.39 J/mol·K^2 for the former and latter model, respectively. Such figures are in excellent agreement with an extrapolation of high field specific heat data where SC is already suppressed by the applied magnetic field. These strongly enhanced Sommerfeld values characterise CePt$_3$Si as a typical heavy fermion compound.

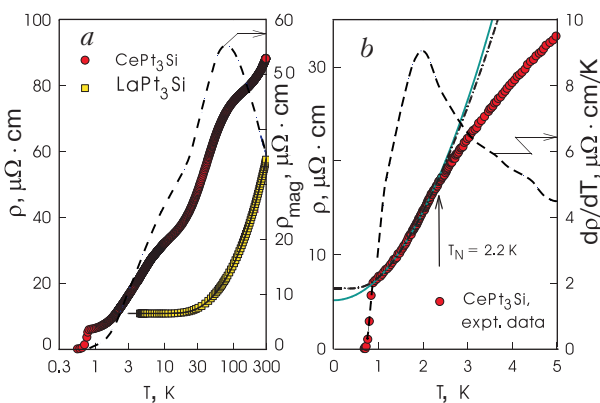Considering Kondo type interactions to be responsible for the significant renormalisation of electrons, the temperature dependent magnetic entropy $S_{mag}(T)$ allows to estimate the Kondo temperature T_K. Applying results derived from the renormalisation group technique [5] for effective spin $1/2$ systems to $S_{mag}(T)$ derived for CePt$_3$Si yields $T_K \approx 7.2$ K. A second possible estimate for T_K follows from the competition of the RKKY interaction and the Kondo effect, which leads to a significant reduction of the specific heat jump at $T = T_N$. Following the procedure developed in Ref. 6 gives $T_K \approx 9$ K, in reasonable agreement with the previous estimate.

The temperature dependent electrical resistivity $\rho(T)$ of CePt$_3$Si is plotted in Fig. 2,*a* together with $\rho(T)$ of isostructural LaPt$_3$Si. $\rho(T)$ of CePt$_3$Si drops to zero from a residual value of 5.8 $\mu\Omega$·cm with $T_c^{mid} = 0.75$ K, thus indicating superconductivity. At high temperatures, $\rho(T)$ is characterised by a negative logarithmic contribution, followed by pronounced curvatures around 75 K and 15 K, which may reflect crystal electric field effects in the presence of Kondo type interactions. Further evaluation of $\rho(T)$ requires knowledge of the phonon contribution ρ_{ph} which, in a first approximation, may be derived from homologous and isotypic LaPt$_3$Si. LaPt$_3$Si is metallic in the temperature range measured and $\rho(T)^{La} = \rho_0^{La} + \rho_{ph}^{La}(T)$ (ρ_0 is residual resistivity) can simply be accounted for in terms of the Bloch Grüneisen model with the Debye temperature $\theta_D \approx 160$ K [solid line, Fig. 2,*a*] and $\rho_0 = 10.7$ $\mu\Omega$·cm. According to Matthiessen's rule, $\rho(T)$ of CePt$_3$Si can be expressed as $\rho(T)^{Ce} = \rho_0^{Ce} + \rho_{ph}^{Ce}(T) + \rho_{mag}(T)$. The temperature dependent magnetic contribution to the resistivity, $\rho_{mag}(T)$, follows then simply from the difference of $\rho(T)^{Ce}$ and $\rho(T)^{La}$, assuming $\rho_{ph}^{Ce} \approx \rho_{ph}^{La}$. Furthermore, ρ_0^{La} is subtracted. $\rho_{mag}(T)$ exhibits a distinct logarithmic contribution for $T > 100$ K; the maximum around 80 K may indicate the overall crystal field splitting of the $j = 5/2$ Ce $4f^1$ state (dashed-line, Fig. 2,*a*, right axis).

Figure 2,*b* exhibits low temperature features of the electrical resistivity of CePt$_3$Si. Besides the onset of superconductivity, there is a distinct change of the slope in $\rho(T)$ around 2 K, which becomes more evident from a $d\rho/dT$ plot [right axis, Fig. 2,*b*]. In the context of the specific heat study, this anomaly is interpreted as a signature of an onset of long range magnetic order. A least squares fit according to $\rho = \rho_0 + AT^2$, reveals the residual resistivity $\rho_0 = 5.2$ $\mu\Omega$·cm and a material dependent constant $A = 2.35$ $\mu\Omega$·cm/K^2.

To account for the magnetically ordered region of CePt$_3$Si in more detail, the above indicated model of Continentino can be adopted for the temperature dependent electrical resistivity, where conduction electrons are scattered on antiferromagnetic magnons [3]

Fig. 2. Temperature dependent electrical resistivity ρ of CePt$_3$Si and LaPt$_3$Si plotted on a logarithmic temperature scale. The magnetic contribution $\rho_{mag}(T)$ (dashed-line) refers to the right axis (*a*). Low temperature details of $\rho(T)$ of CePt$_3$Si. The solid and the dashed-dotted lines are least squares fits (see text) and the dashed-line shows $d\rho(T)/dT$ (*b*).

$$\rho = \rho_0 + A\Delta_{SW}^{3/2}T^{1/2}\exp\left(-\Delta_{SW}/T\right) \times$$

$$\times \left[1 + \frac{2}{3}\left(\frac{T}{\Delta_{SW}}\right) + \frac{2}{15}\left(\frac{T}{\Delta_{SW}}\right)^2\right]. \qquad (2)$$

Again, Δ_{SW} is the spin-wave gap. A least squares fit of Eq. (2) to the experimental data above T_c and below the ordering temperature yields an equally good agreement (dashed-dotted line, Fig. 2,*b*) as the earlier model (solid line, Fig.2,*b*). The spin gap obtained from this fit, $\Delta_{SW} = 2.77$ K, excellently agrees with that value obtained from specific heat analysis.

The coefficient A derived is much larger than usually observed for simple metals like K or Cu, and thus evidences again that the low temperature state of $CePt_3Si$ is dominated by heavy quasiparticles. In fact,
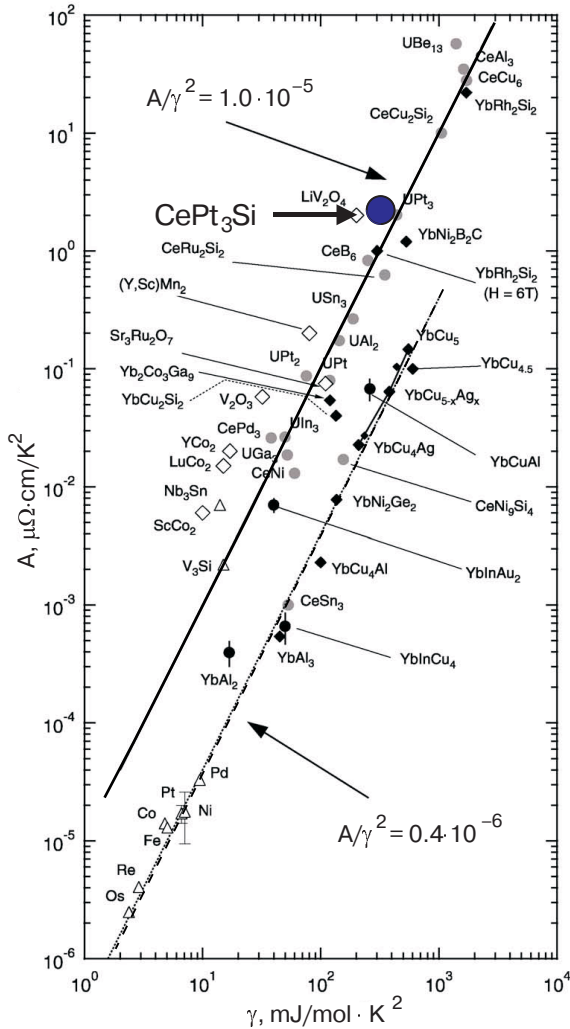
considering the electron−electron interaction in terms of the Barber model indicates $A \propto (N(E_F))^2$, where $N(E_F)$ is the electronic density of states at the Fermi energy. Since also the Sommerfeld value depends on the same quantity, it is naturally to arrange certain systems according their A and γ values. Such a classification was made for the first time by Kadowaki and Woods [7], and many highly correlated electron systems have been shown to satisfy this scheme [8]. A closer inspection yields for the ratio $A/\gamma^2 = 1 \cdot 10^{-5}$ $\mu\Omega \cdot mol^2 \cdot K^2 \cdot mJ^{-2}$. Arranging $CePt_3Si$ in such a Kadowaki Woods plot, see Fig. 3, obviously shows that the present compound is found at the very same site as the unconventional superconductor UPt_3.

Temperature dependent magnetic susceptibility provides information concerning the effective magnetic moments μ_{eff} involved in a particular system, the interaction strength between these moments via the paramagnetic Curie temperature θ_p, and about phase transitions present in a certain sample. Results taken from a SQUID measurement performed at $\mu_0 H = 1$ T are shown in Fig. 4 together with an a.c. susceptibility measurement in the inset of this figure. At elevated temperatures, $\chi(T)$ of $CePt_3Si$ exhibits a Curie−Weiss behavior — and the anomaly around 2.2 K (inset, Fig. 4) indicates the magnetic phase transition. To qualitatively account for the region above about 50 K, a least squares fit according to the modified Curie−Weiss law, i.e.,

$$\chi = \chi_0 + \frac{C}{T + \theta_p} \qquad (3)$$

was applied. χ_0 represents a temperature independent Pauli-like susceptibility and C is the Curie constant.

Fig. 3. A plot of the T^2-coefficient of the electrical resistivity A versus the T-linear specific heat coefficient γ. Solid and dashed lines represent $A/\gamma^2 = 1 \cdot 10^{-5} \mu\Omega \cdot cm \cdot mol^2 \cdot K^2 \cdot mJ^{-2}$ and $A/\gamma^2 = 0.4 \times 10^{-6} \mu\Omega \cdot cm \cdot mol^2 \cdot K^2 \cdot mJ^{-2}$ (figure taken from Ref. [8]).
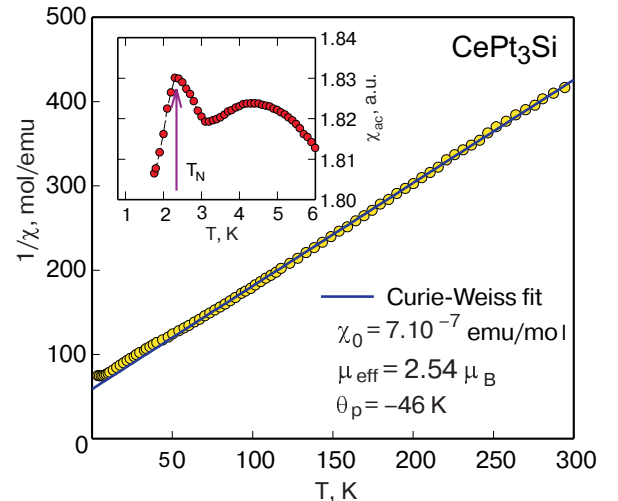

Fig. 4. Temperature dependent susceptibility of $CePt_3Si$ plotted as $1/\chi$ vs T. The solid line is a least squares fit according to the modified Curie−Weiss law. The inset shows the low temperature behaviour deduced from an a.c. susceptibility study (Ref. [9]).

Results of this procedure are shown in Fig. 4 as solid line. The effective magnetic moment deduced from the Curie constant C matches the theoretical value associated with the 3+ state of cerium, thereby inferring a rather stable magnetic moment. The paramagnetic Curie temperature $\theta_p \approx -46$ K is large and negative, being indicative of strong antiferromagnetic interactions. In the Kondo picture, already adopted to explain the large Sommerfeld value γ, the value of θ_p suggests a Kondo temperature of the order of 10 K ($T_K \approx \theta_p / 4$).

Very large values of θ_p ($H \| [100]$ and $H \| [001]$) were also deduced from a previous investigation of single crystalline CePt$_3$Si [4], confirming the substantial antiferromagnetic interaction strength.

For better understanding of the magnetic ground state and expected localized character of Ce $4f$ electrons, neutron inelastic scattering experiments were performed. In order to accurately and reliably determine magnetic scattering from the magnetic moments of Ce, both CePt$_3$Si and LaPt$_3$Si were investigated in powder form under identical conditions. For a proper phonon subtraction, two well-established methods were used [10], yielding almost identical results.

The intensity shown in Fig. 3 for a sample temperature $T = 6.4$ K is expected to be solely of magnetic origin as the phonon contribution has been subtracted from the data. In order to account for the excitations observed, the standard CEF Hamiltonian for Ce^{3+} with C_{4v} point symmetry is considered:

$$H_{CEF} = B_2^0 O_2^0 + B_4^0 O_4^0 + B_4^4 O_4^4. \qquad (4)$$

B_l^m and O_l^m are the CEF parameters and the Steven operators, respectively. Due to CEF effects, the 6-fold degenerate ground state of the Ce^{3+} ions is split in tetragonal symmetry into 3 doublets. Applying Eq. (4) to the data shown in Fig. 5 reveals CEF parameters $B_2^0 = -0.4972$ meV, $B_4^0 = 0.0418$ meV and $B_4^4 = 0.2314$ meV. These parameters are consistent with levels at $\Delta_1 = 13$ and $\Delta_2 = 20$ meV and allow to reasonably well describe magnetic scattering (solid line, Fig. 5). Keeping the CEF parameters unchanged, the data obtained at 94 K are equally well explained. Moreover, the two CEF excitations centred at 13 and 20 meV are also consistent with the heat capacity data as discussed above. We furthermore studied low energy excitations using lower incident energy to find a weak feature around 1.4 meV. The dispersion of that intensity at $T = 5$ K, particularly around $Q = 0.8$ Å^{-1} is a signature for the development of short-ranged magnetic correlations and can be considered as origin of the anomalous behavior of the specific heat above magnetic ordering. At higher temperatures ($T \approx 30$ K) scattering becomes Q-inde-
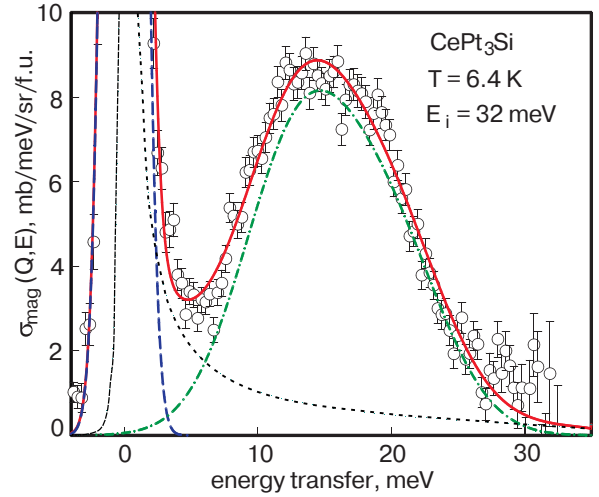

Fig. 5. Magnetic scattering obtained at 6.4 K with the incident energy of 35 meV. The dashed line is for the elastic component with FWHM = 2.4 meV while the short-dashed line represents the quasi-elastic component with FWHM = 0.8 meV. The dashed-dotted line is for the sum of two Lorentzian components centered at 13 and 20 meV with FWHM = 10.0 meV (Ref. [17]).

pendent. This feature is completely absent in non-magnetic LaPt$_3$Si. Differently to our study performed at the instrument HET of ISIS (UK), the inelastic neutron scattering experiment reported in Ref. 4 indicated two CEF peaks at 1.0 and 24 meV. Based on the latter, a set of CEF parameters was deduced, sufficient to account for isothermal magnetisation and the temperature dependent magnetic susceptibility. However, this latter CEF level scheme does not properly describe the temperature dependent magnetic contribution to the specific heat and magnetic entropy. Such a discrepancy is rather serious, since, different to magnetization and susceptibility, not any theoretical model is necessary for the calculation, except basic thermodynamics. In order to get more reliable data for the analysis, particularly at low energy excitations, neutron inelastic measurements with high resolution and low incident energy neutrons are in progress.

2.1. Superconducting properties of CePt$_3$Si

Signs of bulk SC of CePt$_3$Si below $T_c = 0.75$ K are numerous: zero resistivity, diamagnetic signal in the susceptibility, a jump in the specific heat and NMR relaxation rate at T_c.

Substantial information concerning the superconducting state is provided by heat capacity data taken at low temperatures for CePt$_3$Si. Results are shown in Fig. 6 as C_p / T vs. T. The phonon contribution is negligible in the temperature range shown. Besides the already mentioned magnetic phase transition at $T_N = 2.2$ K and the logarithmic contribution above
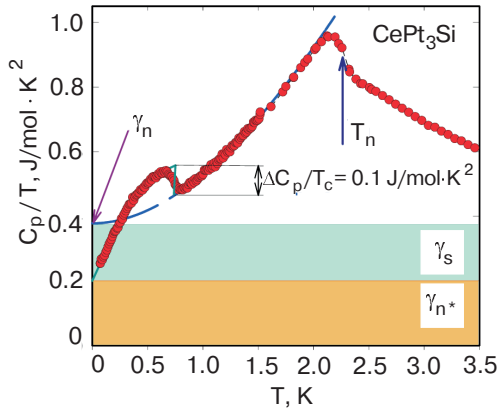
Fig. 6. Temperature dependent specific heat C_p/T of CePt$_3$Si; the dashed line is a T^3 extrapolation of $C_p(T)$ at 0 T.

that temperature, the superconducting transition at $T_c \approx 0.75$ K is the most prominent feature.

The Sommerfeld coefficient $\gamma_n \approx 0.39$ J / mol·K^2 of CePt$_3$Si at zero field, obtained from an extrapolation of the antiferromagnetically ordered region, evidences the large effective masses of the charge carriers involved. The extrapolation shown in Fig. 6 (dashed line) satisfies the basic requirement of superconductivity, the entropy balance between the SC and normal state regions. Another careful extrapolation of the heat capacity of data within the superconducting temperature range towards zero yields about $\gamma_n^* \approx 210$ mJ / mol·K^2. This non-vanishing contribution within the SC state may hint at two mechanisms: not all electrons are involved in the SC condensate, rather, roughly half of them ($\gamma_s \approx \gamma_n^*$) are forming normal state long range magnetic order, which then co-exists with superconductivity on a microscopic scale; a somewhat gapless superconducting state. This would cause finite values of the Sommerfeld constant and power laws of the thermodynamic and transport properties instead of an exponential behavior as in typical BCS systems. The coexistence of both states is evidenced from μSR spectroscopy and a superconducting state with nodes in the gap (gapless at certain sites) is supported by magnetic penetration depth $\lambda(T)$ measurements (see below).

The jump of the specific heat anomaly associated with superconductivity, $\Delta C_p/T|_{T_c} \approx 0.1$ J / mol·K^2, leads to $\Delta C_p/(\gamma_n T_c) \approx 0.25$, which is significantly smaller than the figure expected from the BCS theory ($\Delta C_p/(\gamma T_c) \approx 1.43$). Even using the electronic specific heat coefficient in the SC state, $\gamma_s \approx 0.18(1)$ J / mol·K^2, we obtained $\Delta C_p/(\gamma_s T_c) \approx 0.55$ that is still below the BCS value.

Again, two scenarios may explain the substantial reduction of $\Delta C_p/(\gamma T_c)$ with respect to the BCS value; strongly anisotropic gaps yield a reduced mag-

nitude of $\Delta C_p/(\gamma T_c)$ [11] and not all electrons condense into Cooper pairs while the rest stays essentially normal. This may imply that the electrons responsible for normal state features, such as antiferromagnetic order, coexist with those forming the Cooper pairs. In fact, the finite value of $\gamma_s \approx 0.18$ J / mol·K^2 provides evidence that even at $T = 0$ K a significant portion of the Fermi surface is still not involved in the SC condensate.

Very recently, a specific heat study was performed on a well heat treated polycrystalline CePt$_3$Si sample, revealing two consecutive phase transitions at $T_{c1} \approx 0.8$ and $T_{c2} \approx 0.55$ K. The extreme different field response for both transitions, however, are possibly indicative of two different superconducting states [12].

The upper critical field $H_{c2}(0)$ as well as of the slope $dH_{c2}/dT \equiv H'_{c2}$ are indispensable quantities for the determination of microscopic parameters describing the superconducting state. The temperature and field dependent specific heat $C_p(T,H)$ of CePt$_3$Si is shown for the low temperature range in Fig. 7,a.

The application of magnetic fields reduces T_c, resulting in a rather large change of $dH_{c2}/dT \approx -8.5$, in good agreement with the conclusion drawn from electrical resistivity [see Fig. 7,b]. An extrapolation of $T_c(H)$ towards zero yields $H_{c2}(0) \approx 5$ T, well above the paramagnetic limiting field $H_p \approx 1.1$ T [1]. Furthermore, an estimation of the Sommerfeld coefficient from the high field data gives 0.36 J / mol·K^2, in fair agreement with the value obtained from an extrapolation of the normal state in the zero field data (see Fig. 6). The upturn of C_p/T at lowest temperatures that gets stronger with increasing magnetic field derives from the nuclear contribution of ^{195}Pt.
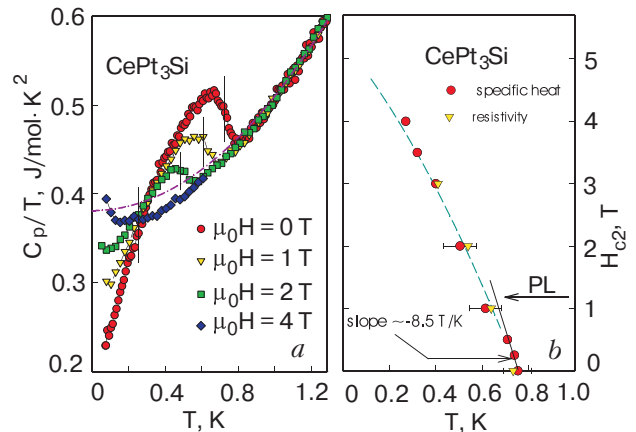

Fig. 7. Temperature dependent specific heat C_p/T of CePt$_3$Si for various values of applied fields; the dashed line is a T^3 extrapolation of $C_p(T)$ at 0 T (*a*). Temperature dependence of the upper critical field H_{c2}. The solid straight line yields $H'_{c2} \approx -8.5$ T/K; the dashed line is a guide to the eyes (Ref. [1]). PL indicates the Pauli−Clogston limiting field (*b*).

In order to derive a set of parameters characterizing the superconducting state of CePt$_3$Si the BCS theory is adopted [13,14]. Although substantial deviations from a spherical Fermi surface are expected for tetragonal CePt$_3$Si, reasonable physical parameters can be expected (compare, e.g., Ref. [14,15]).

Starting parameters are $\gamma_s = 0.18(2)$ J/mol·K^2 (as a lower limit), $H'_{c2} = -8.5$ T/K and $\rho_0 = 5.2$ μΩ·cm.

The effective Fermi surface S_s is then computed (Eq.(2) in Ref. [14]) as $S_s^{cl} \simeq 3.7 \cdot 10^{20}$ m^{-2} within the clean limit and $S_s^{dl} \simeq 3.5 \cdot 10^{20}$ m^{-2} for the dirty limit. Considering the dirty limit only, $H'_{c2} \approx \approx -0.77$ T/K, a value rather low with respect to the experimentally derived slope $H'_{c2} \approx -8.5$ T/K. This indicates that CePt$_3$Si is not a typical dirty limit superconductor. Thus, the further calculations are based on clean limit results.

Combining the Fermi surface with γ_s gives the Fermi velocity $v_F \simeq 5300$ m/s and in the context of the residual resistivity, $\rho_0 = 5.2$ μΩ·cm, a mean free path $l_{tr} \simeq 8 \cdot 10^{-8}$ m can be estimated. The coherence length ξ_0 for $T \to 0$ was obtained from two independent relations. One follows from the BCS equation, $\xi_0 = 0.18\hbar\, v_F/(k_B T_c) \simeq 9.7 \cdot 10^{-9}$ m. A second expression stems from the well known formula $\mu_0 H_{c2} = \Phi_0/(2\pi\xi_0^2)$ yielding $\xi_0 \simeq 8.1 \cdot 10^{-9}$ m, in reasonable agreement with the former.

The evaluation of the Ginzburg Landau parameter $\kappa_{GL} = \lambda/\xi$ requires the knowledge of the thermodynamic critical field $\mu_{0H_c}(0) \simeq 26(2)$ mT which can be calculated from the free energy difference between the superconducting and the normal state:

$$\Delta F(T) = F_n - F_s = \mu_0 H_c^2(T)/2 =$$

$$= \int\limits_{T_c}^{T}\int\limits_{T_c}^{T'} \frac{(C_s - C_n)}{T''}\, dT'' dT'.$$

C_s is obtained from the zero field specific heat and C_n is taken from the T^3 extrapolation as indicated by the dashed line in Fig. 6. With $H_{c2}(0) \approx 5$ T one derives a value for $\kappa_{GL} = H_{c2}(0)/\sqrt{2H_c} \simeq 140$ which, in turn, determines the London penetration depth $\lambda_L(T \to 0) \simeq 1.1 \cdot 10^{-6}$ m. Since the evaluation of the various parameters is based on s-wave models, care has to be taken when using their absolute values; nevertheless the right order of magnitude can be anticipated.

Evaluating Eq. (A.13) of Ref. [14] with $\rho_{max} \approx \approx 100$ μΩ · cm yields $S_{hT} \simeq 3.1 \cdot 10^{21}$ m^{-2}, the Fermi surface at elevated temperatures. The discrepancy between S_s and S_{hT} suggests that only a part of the Fermi surface is involved in forming Cooper pairs while the remaining one engages in normal state magnetic correlations. This finding seems to be convincingly supported from the lessened value of $\Delta C_p/(\gamma T_c)$. In terms of the coexistence of both superconductivity ($T_c = 0.75$ K) and long range magnetic order ($T_N = 2.2$ K), the downsized specific heat jump at T_c may explain, at least partly, that the Fermi surface is likely to be subdivided into a superconducting part (related to γ_s) and a normal state region.

Microscopic evidence for the latter conclusion can be found from zero-field μSR spectroscopy data obtained in the magnetic phase below and above T_c in the magnetic phase (Fig. 8). At temperatures much above T_N, the μSR signal is a characteristic of a paramagnetic state with a depolarization solely arising from nuclear moments. Below T_N the μSR signal indicates that the full sample volume orders magnetically. High statistic runs performed above and below T_c [16] did not show any change of the magnetic signal, supporting the view of a microscopic coexistence between magnetism and SC.

This points to a novel state for SC Ce-based heavy-fermion systems at ambient pressure, for which, to date, magnetism was found to be either absent [18] or strongly competing against SC [19]. The observed coexistence is reminiscent of the situation observed in UPd$_2$Al$_3$ [20], where a model of two independent electron subsets, localized or itinerant, was proposed in view of similar microscopic data [21].

Another microscopic information about the SC state can be obtained from the temperature dependent ^{195}Pt nuclear spin-relaxation rate $1/T_1$ [22]. Results are shown as a $(1/T_1 T)/(1/T_1 T)_{T_c}$ vs. T/T_c plot in Fig. 9 for 8.9 and 18.1 MHz. The relaxation behavior $1/T_1 T$ CePt$_3$Si reminds to a kind of Hebel–Slichter anomaly [23] indicating coherence effects as in conventional BCS SC. The peak height, however, is significantly smaller than that observed for conventional BCS SC and, additionally, shows no field dependence at the 8.9 MHz ($H \sim 1$ T) and 18.1 MHz ($H \sim 2$ T)
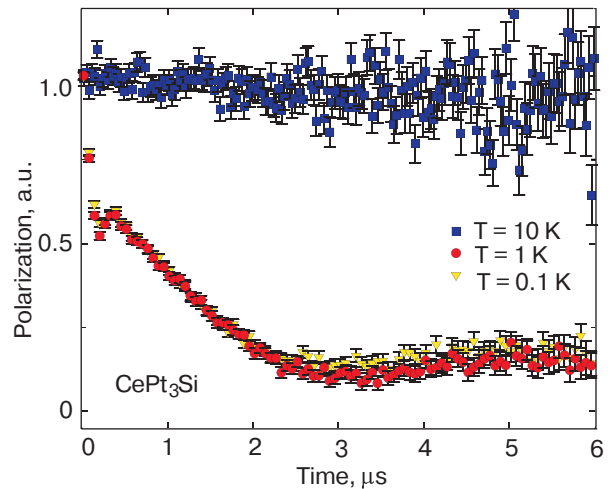

Fig. 8. Zero field depolarisation rate of CePt$_3$Si at various temperatures (Ref. [17]).
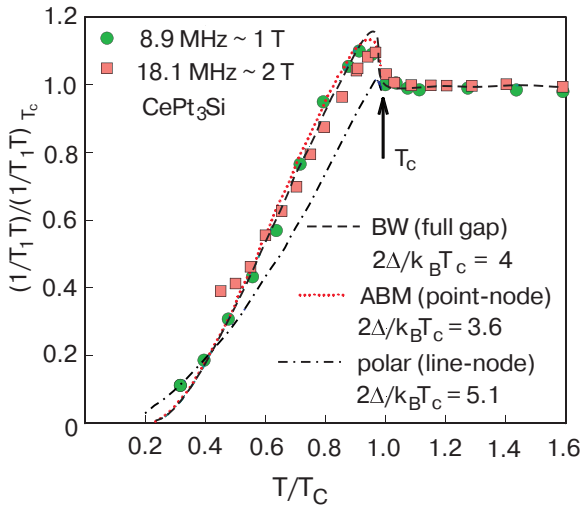
Fig. 9. A plot of $(1/T_1T)/(1/T_1T)_{T_c}$ vs. T/T_c at 8.9 MHz ($H \sim 1$ T) and 18.1 MHz ($H \sim 2$ T). The dashed line is for the Balian-Werthamer model (BW isotropic triplet SC state) with a value of $2\Delta/k_BT_c = 4$. The dotted line assumes a point-node model with $2\Delta/k_BT_c = 3.6$ and the dashed-dotted line represents a fit by a line-node gap model with $2\Delta/k_BT_c = 5.1$ (Ref. [17].

run. Notably, CePt$_3$Si is the first HF SC that exhibits a peak in $1/T_1T$ just below T_c.

$1/T_1T$ at $H \sim 2$ T seems to saturate at low temperature, which can be assigned to the presence of vortex cores where the normal-state region is introduced. $1/T_1T$ at 8.9 MHz ($H \sim 1$ T), however, continues to decrease down to $T = 0.2$ K, the lowest yet measured temperature. Neither an exponential law nor the usual T^3 law, reported for most of the unconventional HF SC (see e.g., Ref. [24] and Refs. therein), is observed for the data down to $T = 0.2$ K ($\approx 0.3T_c$). However, further studies at temperatures below $0.2T_c$ are required to make any definite conclusion on the specific behaviour of $1/T_1$.

The nuclear spin-lattice relaxation rate $1/T_1$ in the superconducting state can be expressed as

$$\frac{1}{T_1} = \frac{2\pi A^2}{\hbar} \int_0^\infty [N_s^2(E) + M_s^2(E)]f(E)[1 - f(E)]dE, \quad (5)$$

N_s is the density of states and describes the distinct features of an isotropic, polar or axial SC state; M_s is the anomalous density of states arising from coherence effects which can be calculated from

$$M_s(E) = \frac{N(0)}{4\pi} \int_0^{2\pi}\int_0^\pi \frac{\Delta(\theta,\varphi)}{\sqrt{E^2 - \Delta^2(\theta,\varphi)}} \sin\theta d\theta d\varphi, \quad (6)$$

with $\Delta(\theta,\varphi)$ the direction dependent energy gap. M_s is expected to only exists in *s*-wave superconductors.
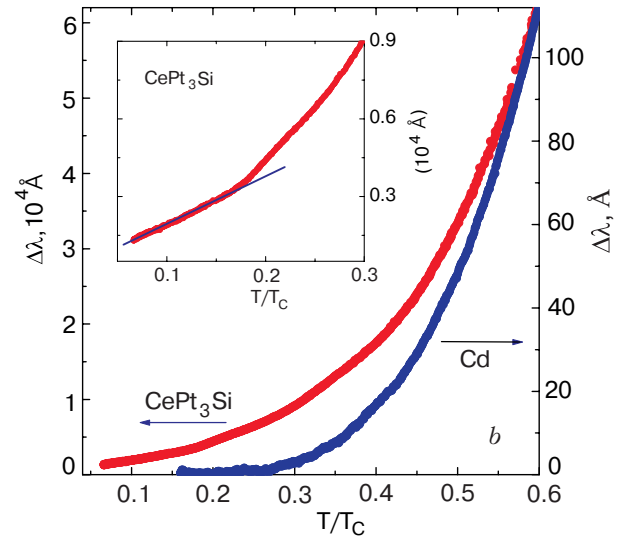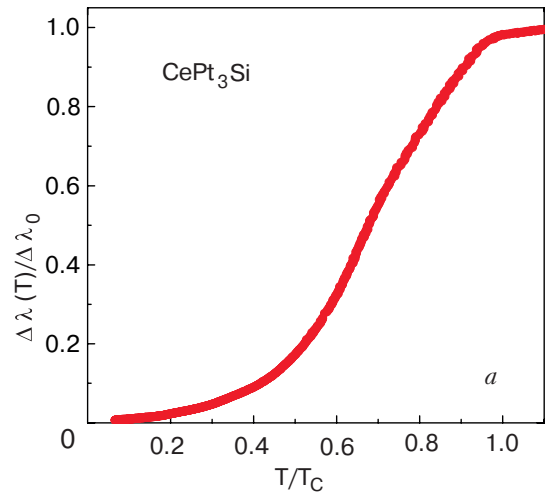

Fig. 10. Normalized variation $\Delta\lambda(T)/\Delta\lambda_0$ versus T/T_c in a polycrystalline CePt$_3$Si sample (*a*). Low-temperature behavior of $\Delta\lambda(T)$ in polycrystalline CePt$_3$Si and Cd samples. $\lambda(T)$ is independent of temperature below $0.28T_c$ in cadmium, as expected for a *s*-wave superconductor. The inset displays a linear low-temperature behavior of $\lambda(T)$ in CePt$_3$Si (*b*).

To account for the relaxation behavior below T_c in noncentrosymmetric CePt$_3$Si, three unconventional models were adopted for a description of the temperature dependence of $1/T_1$ at $H \sim 1$ T. The dashed line in Fig. 9 represents a fit according to the the Balian−Werthamer model (BW isotropic spin-triplet SC state) with $2\Delta/k_BT_c = 3.9$ [25]. Note that the peak of the BW model in $1/T_1T$ originates from the presence of an isotropic energy gap. The dashed-dotted line is a fit using a line-node model with $2\Delta/k_BT_c = 5.1$. The dotted line refers to a point-node model with $2\Delta/k_BT_c = 3.6$. The models used, however, failed to give satisfactory description of the observed temperature dependence of $1/T_1$ over the entire temperature range.

The data seem to start following the line-node model at the lowest measured temperatures. However, the data are described reasonably well by the BW (nodeless) model just below T_c. The experimentally observed peak in $1/T_1T$ would indicate the presence of an isotropic energy gap, even though a coherence effect — inherent for the isotropic spin–singlet s-wave pairing state — is absent.

In almost all previous studies on either conventional and unconventional SC, it was assumed that the crystal has an inversion center, which allows separate consideration of the even (spin–singlet) and odd (spin–triplet) components of the SC order parameter. In CePt₃Si, however, a center of symmetry is absent. Therefore, the novel relaxation behavior found below T_c hints at a possibly new class of a SC state being realized in noncentrosymmetric heavy fermion compounds.

An important probe of the structure of the superconducting energy gap is the temperature dependence of the magnetic penetration depth $\lambda(T)$. Figure 10 shows results, obtained using a tunnel diode oscillator system running at 9.5 MHz, for a polycrystalline CePt₃Si sample at temperatures down to 0.049 K. Figure 10,a depicts the normalized variation of $\Delta\lambda(T)/\Delta\lambda_0$ versus T/T_c in the whole temperature region below T_c. Here $\Delta\lambda(T) = \lambda(T) - \lambda(0.049$ K$)$ and $\Delta\lambda_0$ is the total penetration depth shift. Figure 10,b displays $\Delta\lambda(T)$ vs T/T_c in the low temperature range $T < 0.6T_c$ for polycrystalline CePt₃Si and Cd samples. Cadmium is a classic s-wave superconductor, for which the low temperature dependence of $\lambda(T)$ is exponential. The inset to Fig. 10,b is a close-up of $\Delta\lambda(T)$ vs. T/T_c for the CePt₃Si sample for temperatures $T < 0.3T_c$, where it can be clearly seen that the penetration depth data of the CePt₃Si sample follow a linear temperature behavior below $0.17T_c$. We remark here that the low temperature dependence of $\lambda(T)$ is not affected by the type of sample (single crystal, powder, etc.) in which the measurement is performed, if the sample is of high quality [26–28].

For a clean, local superconductor the penetration depth is given by

$$\frac{\lambda^2(0)}{\lambda^2(T)} = \left[1 + 2\left\langle \int_\Delta^\infty dE \, \frac{\partial f}{\partial E} \frac{E}{\sqrt{E^2 - \Delta^2(T,\theta,\varphi)}} \right\rangle \right]. \quad (7)$$

Here $\langle\dots\rangle$ represents an angular average over the Fermi surface and f is the Fermi function. Evidently the temperature dependence of $\lambda(T)$ depends on the topology of the gap structure. For line nodes in the energy gap the penetration depth is expected to be linear in the low temperature limit, where the temperature dependence of the energy gap can be neglected. As-

suming that CePt₃Si is both a clean ($l > \xi_0$) and a local ($\lambda(0) > \xi_0$) superconductor, as it was discussed above, the penetration depth experimental result points out to the existence of lines of nodes in the structure of the superconducting pairing state and, hence, to unconventional superconductivity in CePt₃Si. For this material with a tetragonal crystal lattice a p-wave pairing symmetry, like $d(k) = \hat{x}k_y - \hat{y}k_x$ proposed earlier by Frigeri et al., will not be consistent with line nodes, because for materials with strong spin-orbit coupling all the spin-triplet states are predicted to have point nodes [29]. Thus, the T linear variation of the penetration depth suggests a d-wave (spin–singlet) type of pairing symmetry in the energy gap.

A broad shoulder in $\Delta\lambda(T)$ just below T_c, like the one observed in Fig. 10,a, is usually associated in polycrystalline samples to inter-grain or proximity effects. However, this effect is not expected to be relevant in the present case, because of the high quality of the polycrystalline sample and the very small measuring magnetic fields (about 5 mOe) [26]. $\Delta\lambda(T)$ for this sample has an inflection point around 0.52 K temperature that is near to the second superconducting transition (0.55 K) recently found in CePt₃Si [12]. Thus, it is tempting to relate the shoulder to this second transition. However, the inflation point —or similar feature— does not seem to be present in preliminary results (obtained by one of the authors) in a sedimented powder sample, where the intrinsic behavior is thought to be more pronounced. Thus, no conclusions can be drawn on the second transition from the present measurements of the penetration depth.

2.3. Symmetry aspects

Time reversal invariance and inversion symmetry are essential ingredients for superconductivity. They allow us to distinguish pairing with spin singlet and spin triplet configuration and even and odd parity. Due to Fermion antisymmetry of the Cooper pair wavefunction these are uniquely combined into even parity spin singlet and odd parity spin triplet pairing states. The formation of Cooper pairs with vanishing total momentum relies on the availability of degenerate electron states of opposite momentum on the Fermi surfaces. It is generally believed that for spin singlet Cooper pairing time reversal invariance provides the necessary conditions, while spin triplet pairing needs additionally an inversion center [2]. The absence of inversion symmetry removes, however, the distinction of even and odd parity and leads immediately to a mixing also of the spin channels [30].

The absence of inversion symmetry gives rise to antisymmetric spin-orbit coupling. In the case of
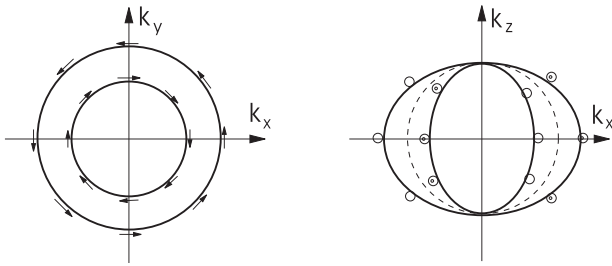
Fig. 11. Fermi surface splitting. The lack of inversion symmetry gives rise to antisymmetric spin-orbit coupling which leads in general to a splitting of the spin degeneracy of the electronic states. The figure depicts schematically the splitting of the Fermi surfaces for the generating point group C_{4v} CePt$_3$Si. The spinor states are k-dependent in the way that the spin quantization axes lie perpendicular to the Fermi surface and the z-axis with the spin pointing in opposite direction for the two Fermi surfaces. This feature is essential for the possible spin configuration of the pairing states which can be constructed from two electrons on the same Fermi surface.

CePt$_3$Si the generating point group is C_{4v} which implies that there is no reflection symmetry $z \to -z$ where z is the fourfold tetragonal rotation axis. This is incorporated into band structure by a Rashba-like term

$$\epsilon_{\mathbf{k}} \sigma_0 \to \epsilon_{\mathbf{k}} \sigma_0 + \alpha(\hat{z} \times \mathbf{k})\sigma \qquad (8)$$

with σ_0 as unit matrix and σ as the Pauli matrices in the electron spinor space. The electron bands split into two yielding two different Fermi surfaces with opposite spinor orientation as depicted in Fig. 11. Obviously there is now a clear restriction on the possible spin configurations for zero momentum Cooper pairs

The mixing of the spin singlet and spin triplet channel for this electron band structure leads to an non-vanishing spin susceptibility at $T = 0$ in any case [30−32]. Thus the absence of paramagnetic limiting would be naturally explained. It was suggested, however, by Kaur and collaborators that in high magnetic fields perpendicular to the z-axis a novel superconducting phase with a helical order parameter could be realized which would leave its traces in the temperature dependence of the upper critical field [33].

So far the symmetry of the order parameter remains an open question. However, theoretical considerations suggest that the lack of inversion symmetry introduces several complications in the microscopic discussion of superconductivity [30,31,34−39].

3. Summary

We summarize that non-centrosymmetric CePt$_3$Si is a heavy fermion SC with $T_c = 0.75$ K that orders magnetically at $T_N = 2.2$ K. Specific heat, NMR and μSR studies indicate that superconductivity and long range magnetic order coexist on a microscopic scale and may be originated by two different sets of electrons. The NMR relaxation rate $1/T_1$ shows unexpected features which were neither found before in conventional nor in heavy fermion SC, indicative of very unusual shapes of the SC order parameter. Unconventional SC is backed also by the present penetration depth studies. In fact, the various theoretical scenarios developed for this compound support these conclusions.

1. E. Bauer, G. Hilscher, H. Michor, Ch. Paul, E.W. Scheidt, A. Gribanov, Yu. Seropegin, H. Noel, M. Sigrist, and P. Rogl, *Phys. Rev. Lett.* **92**, 027003 (2004).

2. P.W. Anderson, *Phys. Rev.* **B30**, 4000 (1984).

3. M.A. Continentino, S.N. de Medeiros, M.T.D. Orlando, M.B. Fontes, and E.M. Baggio-Saitovitch, *Phys. Rev.* **B64**, 012404 (2001).

4. N. Metoki, K. Kaneko, T.D. Matsuda, A. Galatanu, T. Takeuchi, S. Hashimoto, T. Ueda, R. Settai, Y. Onuki, and N. Bernhoeft, *J. Phys.: Cond. Mat.* **16**, L207 (2004).

5. H.U. Desgranges and K.D. Schotte, *Phys. Lett.* **A91**, 240 (1982).

6. M. Besnus, M.J. Braghta A. Hamdaoui, and A. Meyer, *J. Magn. Magn. Mater.* **104−107**, 1385 (1992).

7. K. Kadowaki and S.B. Woods, *Solid State Commun.* **58**, 507 (1986).

8. N. Tsujii, K. Yoshimura, and K. Kosuge, *J. Phys.: Condens. Matter* **15**, 1993 (2003).

9. E. Bauer, R. Lackner, G. Hilscher, H. Michor, M. Sieberer, A. Eichler, A. Gribanov, Y. Seropegin, and P. Rogl, *J. Phys.: Cond. Mat.* **17**, (2005) in press.

10. D.T. Adroja, J.G. Park, K.A. McEwen, N. Takeda, M. Ishikawa, and J.-Y. So, *Phys. Rev.* **B68**, 094425 (2003).

11. A.P. Makenzie and Y. Maeno, *Rev. Mod. Phys.* **75**, 657 (2003).

12. E.W. Scheidt, F. Mayr, G. Eickerling, P. Rogl, and E. Bauer, *J. Phys.: Cond. Mat.* **17**, L121 (2005).

13. See, for example M. Tinkham, *Introduction to Supercondcutivity*, McGraw-Hill, New York (1975).

14. U. Rauchschwalbe, *Physica* **147B**, 1 (1987).

15. R. Movshovich, M. Jaime, J.D. Thompson, C. Petrovic, Z. Fisk, P.G. Pagliuso, and J.L. Sarrao, *Phys. Rev. Lett.* **86**, 5152 (2001).

16. A. Amato, E. Bauer, and C. Baines, *Phys. Rev.* **B** (2005) in press.

17. E. Bauer, G. Hilscher, H. Michor, M. Sieberer, E.W. Scheidt, A. Gribanov, Yu. Seropegin, P. Rogl, A. Amato, W.Y. Song, J.-G. Park, D.T. Adroja, M.

Nicklas, G. Sparn, M. Yogi, and Y. Kitaoka, *Physica B* (2005) in press.

18. C. Petrovic, R. Movshovich, M. Jaime, P.G. Pagliuso, M.F. Hundley, J.L. Sarrao, Z. Fisk, and J.D. Thompson, *Europhys. Lett.* **53**, 354 (2001).

19. G.M. Luke, A. Keren, K. Kojima, L.P. Le, B.J. Sternlieb, W.D. Wu, Y.J. Uemura, Y. Onuki, and T. Komatsubara, *Phys. Rev. Lett.* **73**, 1853 (1994).

20. R. Feyerherm, A. Amato, C. Geibel, F.N. Gygax, P. Hellmann, R.H. Heffner, D.E. MacLaughlin, R. Müller–Reisener, G.J. Nieuwenhuys, A. Schenck, and F. Steglich, *Phys. Rev.* **B56**, 699 (1997).

21. R. Caspary, P. Hellmann, M. Keller, G. Sparn, C. Wassilew, R.Köhler, C. Geibel, C. Schank, F. Steglich, and N.E. Phillips, *Phys. Rev. Lett.* **71**, 2146 (1993)

22. M. Yogi, Y. Kitaoka, S. Hashimoto, T. Yasuda, R. Settai, T.D. Matsuda, Y. Haga, Y. Onuki, P. Rogl, and E. Bauer, *Phys. Rev. Lett.* **93**, 027003 (2004).

23. L.C. Hebel and C.P. Slichter, *Phys. Rev.* **107**, 901 (1957).

24. H. Tou, Y. Kitaoka, K. Asayama, C. Geibel, C. Schank, and F. Steglich, *J. Phys. Soc. Jpn.* **64**, 725 (2003).

25. R. Balian and N.R. Werthamer, *Phys. Rev.* **131**, 1553 (1963).

26. R.B. Goldfarb, M. Lelental and C.A. Thompson, in: *Magnetic Susceptibility of Superconductors and Other Spin Systems*, R.A. Hein (ed.) Plenum Press, New York (1991), p. 49.

27. T. Xiang, C. Panagopoulos, and J.R. Copper, *Int. J. Mod. Phys.* **B12**, 1007 (1998); C. Panagopoulos, *Phys. Rev. Lett.* **79**, 2320 (2097).

28. I. Bonalde, W. Brämer–Escamilla, and E. Bauer, to be published.

29. M. Sigrist and K. Ueda, *Rev. Mod. Phys.* **63**, 239 (1991).

28. F. Manzano, A. Carrington, N.E. Hussey, S. Lee, A. Yamamoto and S. Tajima, *Phys. Rev. Lett.* **88**, 047002 (2002).

30. L.P. Gor'kov and E.I. Rashba, *Phys. Rev. Lett.* **87**, 037004 (2001).

31. P.A. Frigeri, D.F. Agterberg, and M. Sigrist, *New J. Phys.* **6**, 931 (2004).

32. L.N. Bulaevski, A.A. Guseinov, and A.I. Rusinov, *Sov. Phys. JETP* **44**, 1243 (1976).

33. R.P. Kaur, D.F. Agterberg, and M. Sigrist, *cond-mat/0408149.*

34. K.V. Samokhin, E.S. Zijlstra, and S.K. Bose, *Phys. Rev.* **B69**, 094514 (2004).

36. P.A. Frigeri, D.F. Agterberg, A. Koga, and M. Sigrist, *Phys. Rev. Lett.* **92**, 097001 (2004).

37. V.P. Mineev, *Int. J. Mod. Phys.* **B18**, 2963 (2004).

38. I.A. Sergienko and S. Curnoe, *Phys. Rev.* **B70**, 144522 (2004).

39. S.S. Saxena and P. Monthoux, *Nature* **427**, 799 (2004).